ORIGINAL PAPER

The Analytical Model for Horizontal Wellbore Stability in Anisotropic Shale Reservoir

Yi Ding · Xiangjun Liu · Pingya Luo

Abstract Wellbore collapse is a frequent problem during drilling in shale gas reservoir, restricting efficient exploration of shale gas. Due to the presence of bedding plane, conventional homogeneity model is inappropriate to conduct wellbore stability analysis in shale reservoir. Therefore, in this study, under the influence of bedding plane, stress distributions including in situ stress components, pore pressure, seepage stress have been calculated. Meanwhile, shale strength is expressed using the Jaeger's criterion, which assumes shale is isotropic body with one group of weak planes. In combination with stress distribution and shale strength, an analytical model has been developed to investigate wellbore failure region. By using this model, influence factors of wellbore stability have been fully analyzed. Results demonstrate that the difference between bedding plane and rock matrix will modify in situ stress components, transport equations and rock mechanical properties around wellbore. As a result, there are heterogeneous distributions of shale strength and stress state. When the shear failure along bedding plane happens, shale strength has clearly reduction and breakout region has increment, changed from two-lobed failure to four-lobed failure shape. The different intersections between bedding plane and wellbore make variable anisotropy in wellbore plane, modifying the pore pressure propagation and seepage stress distribution. When the bedding plane angle in wellbore plane is low or high value, shear failure along bedding plane doesn't happen and wellbore stability is depended on rock matrix strength. For middle bedding plane angle, failure region clearly increases and shear failure along bedding plane occurs, aggravating the instability. Furthermore, drilling fluid reduces shale strength, thus increasing region area and changing failure mode. This drilling fluid impact is strong in initial stage and becomes stable after 96 h. By having comprehensive investigation on bedding plane influence, findings in this study are advantageous for drilling operations in shale reservoir.

Keywords Shale reservoir · Wellbore stability · Bedding plane · Failure region

Y. Ding (✉) · X. Liu · P. Luo
State Key Laboratory of Oil and Gas Reservoir Geology
and Exploitation, Southwest Petroleum University,
Chengdu 610500, Sichuan, People's Republic of China
e-mail: dingswpu@foxmail.com

X. Liu
e-mail: liuxiangjunswpl@163.com

P. Luo
e-mail: luopingyaswpu@163.com

List of Symbols

$[\varepsilon]$	Vector of strain components
$[\sigma]$	Vector of stress components
$[A]$	Compliance matrix
E_h	Young modulus along bedding plane (GPa)

E_v	Young modulus perpendicular to bedding plane (GPa)	K^{11}	Membrane efficiency (m^3 s/kg)
v_h	Poisson ratio along bedding plane	n	Mole number of solute ions
v_v	Poisson ratio perpendicular to bedding plane	R	Perfect gas constant
		T	Temperature (°C)
$\sigma_x^b,\sigma_y^b,\sigma_z^b$	Normal effective stresses in x, y and z directions respectively (MPa)	C_s	Solute concentration of pore fluid (mol/L)
		ρ	Fluid density (g/cm^3)
$\tau_{xy}^b,\tau_{xz}^b,\tau_{yz}^b$	Effective shear stresses in xy, xz and zy directions respectively (MPa)	t	Time (s)
		p_0'	Atmospheric pressure (MPa)
		ρ_0	Density of fluid (g/cm^3)
$\sigma_x^o,\sigma_y^o,\sigma_z^o$	Original normal in-situ stress components in x, y and z directions respectively (MPa)	c_ρ	Fluid compressibility (MPa^{-1})
		D^{eff}	Diffusion coefficient in homogeneity (m^2/s)
$\tau_{xy}^o,\tau_{xz}^o,\tau_{yz}^o$	Original in-situ shear stress components in xy, xz and yz directions respectively (MPa)	r_w	Radius of borehole (m)
		θ	Circumferential angle (°)
		C_m	Solute concentration of the drilling fluid (mol/L)
$a_{31},a_{32},a_{33},a_{35},a_{36},a_{33}$	Coefficients of the compliance matrix [A]	C_o	Original solute concentration of fluid in formation (mol/L)
μ_1,μ_2,μ_3	Roots of characteristic equations	p_o	Original pore pressure (MPa)
$\lambda_1,\lambda_2,\lambda_3$	Related coefficient of these roots	$\sigma_r^s,\sigma_\theta^s,\sigma_z^s$	Radial, circumferential and axis seepage stress, respectively (MPa)
p_w	Mud pressure (MPa)	a_b	Biot coefficient
Re	Notation for the real part of the complex expressions in the brackets	v	Poisson's ratio
		$\sigma_r,\sigma_\theta,\sigma_z$	Radial, hoop and axial stresses in wellbore coordinate, respectively (MPa)
$\sigma_v,\sigma_H,\sigma_h$	Vertical, maximum horizontal and minimum horizontal in situ stress (MPa)		
		$\tau_{\theta z},\tau_{r\theta},\tau_{rz}$	Components of shear stress in wellbore coordinate (MPa)
Ω	Wellbore inclination (°)	c_f	Cohesion of failure plane (MPa)
Ψ	Wellbore azimuth (°)		
K_{ij}^1	Equivalent hydraulic coefficient	φ_f	Internal friction angle of failure plane (°)
K_{11},K_{22}	Hydraulic coefficient parallel and vertical to bedding plane respectively	β_f	Included angle between the direction of maximum principal stress and the direction normal to failure plane (°)
D_{11},D_{22}	Diffusion coefficient parallel and vertical to bedding plane respectively	c_w,c_0	Cohesion of bedding plane and rock matrix respectively (MPa)
J_v	Water flux	φ_w,φ_0	Internal friction angle of bedding plane and rock matrix respectively (°)
K^1	Hydraulic coefficient in homogeneity (m^3 s/kg)		

β_0	Included angle between the direction of maximum principal stress and the direction normal to plane across rock matrix (°)
β_w	Included angle between the direction of maximum principal stress and the direction normal to bedding plane (°)

1 Introduction

With significant development of oil–gas industry, conventional resources cannot satisfy global demands. As a resource with extremely high potential, shale gas has attracted huge attention globally in petroleum engineering (Qian et al. 2003; Yuan et al. 2015). Whereas, in the exploitation of shale gas, wellbore collapse occurs frequently in shale formation, lengthening the drilling process and incurring huge expenses (Ma and Chen 2014; Al-Ajmi 2012). In order to solve the problem of borehole instability, different solutions have been proposed. As a common approach, high mud pressure is often applied to keep wellbore stability (Mody and Hale 1993). In the case of shale with strong hydration, drilling fluids having different inhibitors are produced and hydration evaluation methods have been established (Zhong et al. 2011; Deville et al. 2011; Liu et al. 2019). Meanwhile, numerous wellbore stability models are developed to analyze its influence factors, like pore pressure, wellbore track, drilling fluid and so on (Wang et al. 2012; Meier et al. 2015; Dokhani et al. 2015).

In conventional wellbore stability modeling, the formation is assumed to be linear elastic and isotropic (Aadnoy 1987). Whereas, it is well-known that bedding planes and lamination are the geological characteristics of shale reservoir, influencing the evaluation of borehole stability. The naturally self-contained bedding plane is able to make stress distribution and rock strength different from homogeneity. Based on the transverse isotropy and elastic linear theory, the stress distribution in layered formation was established by Lekhnitskii (1963). For shale strength with bedding planes, experimental studies

have illustrated that slip failure occurs along weak planes with certain stress states, which obviously reduces the rock strength. Based on that, single weak plane criterion has been used to establish mathematical models of wellbore stability (Yu 2002; Dokhani et al. 2016).

According to above statements, we can find out that lots of scholars performed researches about the influence of bedding plane on shale mechanical property. However, bedding plane and rock matrix also have difference in physical property, leading to the anisotropy of permeability and diffusion ability (He et al. 2017). This anisotropy will affect transport equations. Consequently, pore pressure and seepage stress around wellbore will be modified, and totally different from homogeneity situation (Ekbote and Abousleiman 2006). This stress modification can further change failure region around wellbore (Zoback et al. 1985).

Thus, we can conclude that bedding plane can simultaneously put impact on shale strength, in situ stress components, pore pressure, seepage stress. Currently, researches merely include parts of these influences. For instance, Liang et al. (2014), Chen et al. (2015) conducted study on influence of shale strength with bedding plane on wellbore stability. Zhou et al. (2018) considered rock strength and seepage stress with bedding plane, offering a new wellbore stability model for laminated formation. Ma and Chen (2015) established a wellbore stability model by considering shale strength and pore pressure with bedding plane. Kanfar et al. (2017) built a numerical solution for in situ stress components and pore pressure around wellbore with bedding plane. Since shale strength, in situ stress components, pore pressure, seepage stress are all affected by bedding plane, a comprehensive research should be conducted to have fully investigation on wellbore stability in shale reservoir.

Therefore, in this paper, take horizontal wellbore as an example, by considering the anisotropy feature caused by bedding plane, calculated equations for shale strength, in situ stress components, pore pressure and seepage stresses in anisotropic medium have been established. Then, in combination with these equations, a new analytical model has been developed to analyze failure region and evaluate wellbore stability. This study gives systematic wellbore stability analysis

and its outcomes can offer theoretical reference for drilling in shale reservoir.

2 Model of Wellbore Stability in Shale Reservoir with Anisotropy

2.1 In Situ Stress Components Around Wellbore

The parallel bedding plane makes shale formation become a typical layered medium, which can be regarded as transverse isotropy, shown as Fig. 1. In the borehole coordinate, the constitutive equation between stress and strain can be expressed as Eq. (1) and Eq. (2) using Hooke's law.(Ding et al. 2018).

$$[\varepsilon] = [A][\sigma] \tag{1}$$

$$[A] = \begin{bmatrix} \frac{1}{E_h} & -\frac{v_h}{E_h} & -\frac{v_v}{E_v} & 0 & 0 & 0 \\ -\frac{v_h}{E_h} & \frac{1}{E_h} & -\frac{v_v}{E_v} & 0 & 0 & 0 \\ -\frac{v_v}{E_v} & -\frac{v_v}{E_v} & \frac{1}{E_v} & 0 & 0 & 0 \\ 0 & 0 & 0 & \frac{1}{E_h}+\frac{1}{E_v}+2\frac{v_v}{E_h} & 0 & 0 \\ 0 & 0 & 0 & 0 & \frac{1}{E_h}+\frac{1}{E_v}+2\frac{v_v}{E_h} & 0 \\ 0 & 0 & 0 & 0 & 0 & \frac{2(1+v_h)}{E_h} \end{bmatrix} \tag{2}$$

Stress, strain and displacement expressions of rock around wellbore are limited to equilibrium equations, constitutive relations and boundary conditions (Rizzo and Shippy 1970; Gupta and Zaman 1999). Thus, for
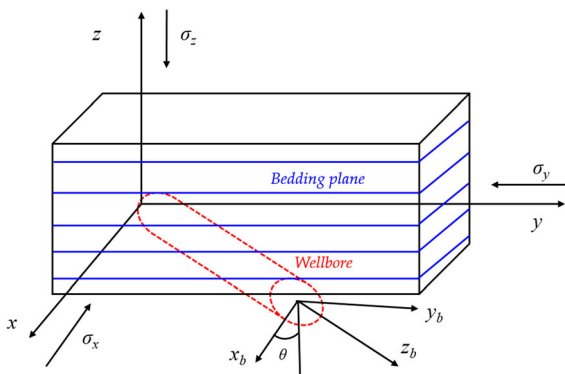
lamination medium, these researches give stress distribution around borehole, shown as Eq. (3). Also, note that the expression of reciprocal equation (ϕ_k) can be acquired from research of Amadei (1984).

$$\begin{cases} \sigma_x^b = \sigma_x^o + 2\mathrm{Re}\left[\mu_1^2\phi_1'(z_1) + \mu_2^2\phi_2'(z_2) + \mu_3^2\lambda_3\phi_3'(z_3)\right] \\ \sigma_y^b = \sigma_y^o + 2\mathrm{Re}\left[\phi_1'(z_1) + \phi_2'(z_2) + \lambda_3\phi_3'(z_3)\right] \\ \sigma_z^b = \sigma_z^o - \dfrac{1}{a_{33}}\left(a_{31}\sigma_{x,h} + a_{32}\sigma_{y,h} + a_{34}\tau_{yz,h}\right. \\ \qquad\quad \left. + a_{35}\tau_{xz,h} + a_{36}\tau_{xy,h}\right) \\ \tau_{xy}^b = \tau_{xy}^o - 2\mathrm{Re}\left[\mu_1\phi_1'(z_1) + \mu_2\phi_2'(z_2) + \mu_3\lambda_3\phi_3'(z_3)\right] \\ \tau_{xz}^b = \tau_{xz}^o + 2\mathrm{Re}\left[\lambda_1\mu_1\phi_1'(z_1) + \lambda_2\mu_2\phi_2'(z_2) + \mu_3\phi_3'(z_3)\right] \\ \tau_{yz}^b = \tau_{yz}^o - 2\mathrm{Re}\left[\lambda_1\phi_1'(z_1) + \lambda_2\phi_2'(z_2) + \phi_3'(z_3)\right] \end{cases} \tag{3}$$

For original in-situ stress components, its distribution should be derived from in-situ stress by conducting wellbore coordinate transformation (Fig. 2). After this coordinate transformation, formulation of original in situ stress components in wellbore coordinate is written as Eq. (4) (Chen et al. 2003). Inserting Eq. (4) into Eq. (3), in situ stress components around wellbore in laminated formation can be obtained.

Fig. 1 Schematic of horizontal wellbore in formation with transverse isotropy
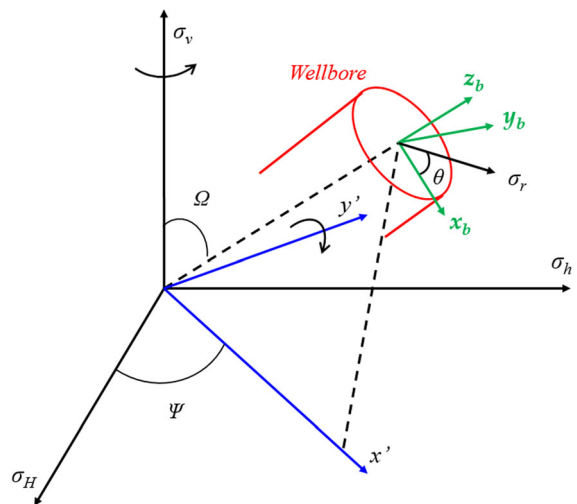

Fig. 2 Schematic of coordinate transformation

$$\begin{cases} \sigma_x^o = \sigma_H \cos^2 \Omega \cos^2 \Psi + \sigma_h \cos^2 \Omega \sin^2 \Psi + \sigma_v \sin^2 \Omega \\ \sigma_y^o = \sigma_H \sin^2 \Psi + \sigma_h \cos^2 \Psi \\ \sigma_z^o = \sigma_H \sin^2 \Omega \cos^2 \Psi + \sigma_h \sin^2 \Omega \sin^2 \Psi + \sigma_v \cos^2 \Omega \\ \tau_{xy}^o = -\sigma_H \cos \Omega \cos \Psi \sin \Psi + \sigma_h \cos \Omega cos \Psi \sin \Psi \\ \tau_{yz}^o = -\sigma_H \sin \Omega \cos \Psi \sin \Psi + \sigma_h \sin \Omega cos \Psi \sin \Psi \\ \tau_{xz}^o = \sigma_H \cos \Omega \sin \Omega \cos^2 \Psi + \sigma_h \cos \Omega \sin \Omega \sin^2 \Psi \\ \qquad - \sigma_v \sin \Omega \cos \Omega \end{cases}$$

$$(4)$$

To clarify the influence of bedding plane on in situ stress components, with certain horizontal wellbore azimuth ($\Omega = 90°$ $\Psi = 0 °$), take circumferential stress as an indicator, stress distribution around wellbore in varying Young modulus anisotropy (E_v/E_h), Poisson ratio anisotropy (v_v/v_h) and bedding plane occurrence have been computed, shown in Figs. 3, 4. It can be seen that the overall changing trend is constant, meaning that circumferential stress grows with increasing circumferential angle. For the circumferential stress in different anisotropy of elastic parameters, comparing Young modulus and Poisson ratio, effecting degree of Young modulus is clearly larger. When it comes to bedding plane inclination and azimuth, they have different influence mechanisms on stress. In the regions close to 0°or 90°, stress grows with increasing inclination and decreasing azimuth. On the other hand, in the middle of circumferential angle, this influence is reverse, indicating low inclination and high azimuth represent large stress.

2.2 Pore Pressure Propagation Around Wellbore

2.2.1 Permeability Characteristics in the Anisotropy Formation

It has been noticed that the bedding plane and rock matrix have different physical properties (Zhang et al. 2018). In particular, compared to rock matrix, bedding plane normally has comparatively stronger permeability and diffusion ability, thus making water and solute transport have anisotropy characteristic. Consequently, transport equations of pore pressure will be changed. In order to express this anisotropy, we establish plane model of pore pressure transport in anisotropy medium, shown as Fig. 5. The a is included angle between bedding plane and x axis. For certain fluid (drilling fluid and formation fluid), due to the difference between bedding plane and rock matrix, parameters of water osmosis and solute diffusion, like hydraulic coefficient and diffusion coefficient, are related to bedding plane angle (Lomba et al. 2000). Based on that, the equation of equivalent hydraulic coefficient in shale formation is written as (Yang et al. 2014):

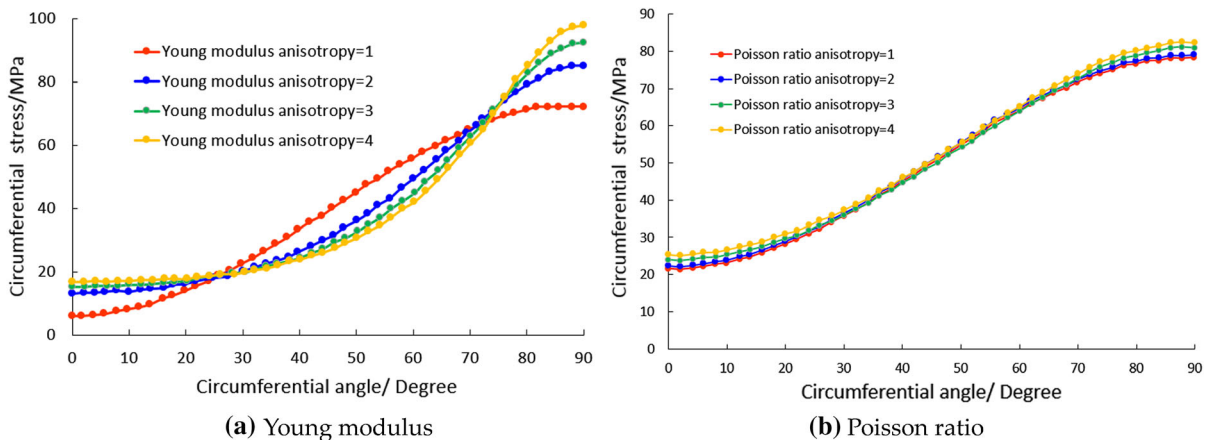$$K_{ij}^1 = \begin{bmatrix} K_{xx} & K_{xy} \\ K_{yx} & K_{yy} \end{bmatrix}$$

$$(5)$$

(a) Young modulus

(b) Poisson ratio

Fig. 3 Circumferential stress of in situ stress components with different elastic parameters
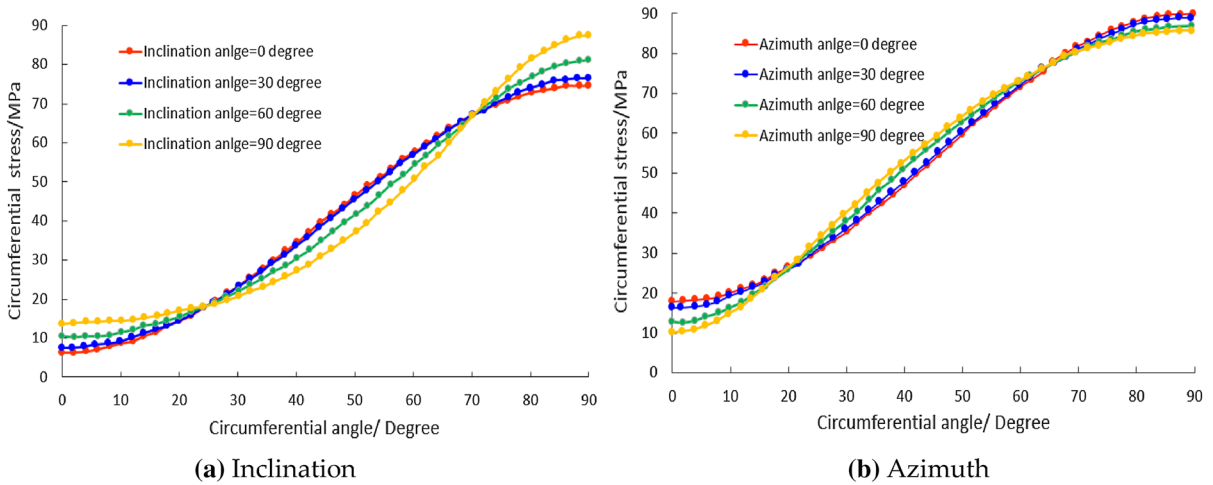
(a) Inclination

(b) Azimuth

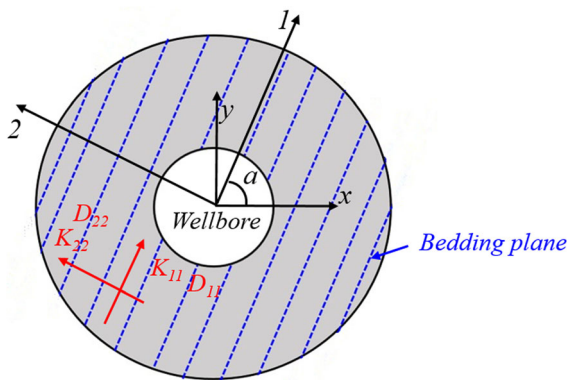**Fig. 4** Circumferential stress of in situ stress components with bedding plane occurrence

Fig. 5 Hydraulic and diffusion coefficient in shale with bedding plane

$$
\begin{cases}
K_{xx} = \dfrac{K_{11} + K_{22}}{2} + \dfrac{K_{11} - K_{22}}{2} \cos 2a \\[2mm]
K_{xy} = K_{yx} = \dfrac{K_{11} - K_{22}}{2} \sin 2a \\[2mm]
K_{yy} = \dfrac{K_{11} + K_{22}}{2} - \dfrac{K_{11} - K_{22}}{2} \cos 2a
\end{cases}
\tag{6}
$$

For the same method, equivalent diffusion coefficient tensor (D_{ij}^{eff}) is expressed as Eqs. (7), (8).

$$
D_{ij}^{eff} = \begin{bmatrix} D_{xx} & D_{xy} \\ D_{yx} & D_{yy} \end{bmatrix}
\tag{7}
$$

$$
\begin{cases}
D_{xx} = \dfrac{D_{11} + D_{22}}{2} + \dfrac{D_{11} - D_{22}}{2} \cos 2a \\[2mm]
D_{xy} = D_{yx} = \dfrac{D_{11} - D_{22}}{2} \sin 2a \\[2mm]
D_{yy} = \dfrac{D_{11} + D_{22}}{2} - \dfrac{D_{11} - D_{22}}{2} \cos 2a
\end{cases}
\tag{8}
$$

By using the above equations, hydraulic coefficient and diffusion coefficient in laminated medium can be computed, shown as Figs. 6, 7. Curves in these figures depict clear variation of hydraulic and diffusion coefficient around wellbore. It is important to note that no matter how bedding plane angle changes, those two coefficients reach maximum along bedding plane, indicating bedding plane is the easiest path for water invading and solute diffusion. When the direction gradually changes from parallel bedding plane to vertical bedding plane, hydraulic and diffusion coefficient show decline. Maximum to minimum ratio of hydraulic and diffusion coefficient are 2.75 and 1.56 respectively.

2.2.2 The Propagation of Pore Pressure

The pore pressure propagation is related to water and solute transport. Based on Darcy law and chemical potential theory, water transport equation can be given by (Yu et al. 2003):

$$
J_v = -K^1 \cdot \nabla p - nRTK^{11} \cdot \nabla C_s
\tag{9}
$$

In water transport, considering mass conservation law and compressibility of fluid in pore, mass equation can be expressed as:
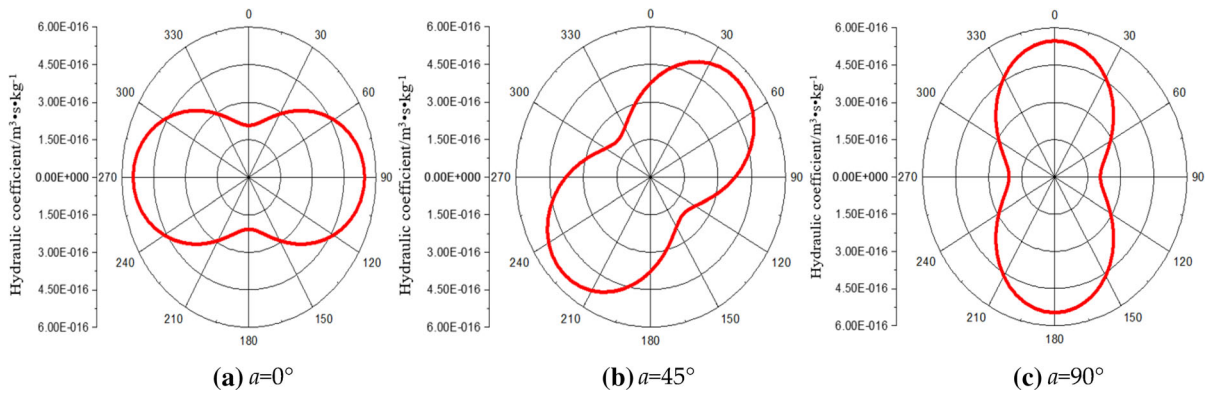
(a) $a=0°$ **(b)** $a=45°$ **(c)** $a=90°$

Fig. 6 Hydraulic coefficient in shale with bedding plane angle

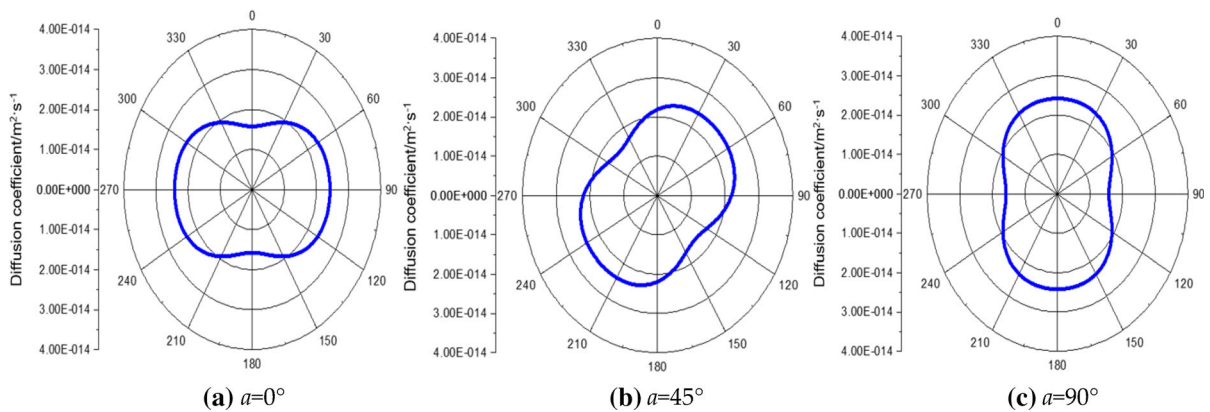**(a)** $a=0°$ **(b)** $a=45°$ **(c)** $a=90°$

Fig. 7 Diffusion coefficient in shale with bedding plane angle

$$\frac{\partial p}{\partial t} + \frac{1}{c_\rho} \nabla J_v + J_v \cdot \nabla p = 0 \qquad (10)$$

Substituting Eq. (10) into Eq. (9):

$$\frac{\partial p}{\partial t} - \frac{1}{c_\rho} \nabla (K^1 \cdot \nabla p) - \frac{nRt}{c_\rho} \nabla (K^{11} \cdot \nabla C_s) = 0 \qquad (11)$$

Incorporating the anisotropy of hydraulic coefficient into the Eq. (11), it can be rewritten in polar coordinate, shown as:

$$\frac{\partial p}{\partial t} = \frac{1}{c_\rho} \left[\frac{1}{r}\frac{\partial}{\partial r}\left(K_{ij}^1 r \frac{\partial p}{\partial r}\right) + \frac{1}{r^2}\frac{\partial}{\partial \theta}\left(K_{ij}^1 \frac{\partial p}{\partial \theta}\right) \right]$$
$$+ \frac{nRT}{c_\rho}\left[\frac{1}{r}\frac{\partial}{\partial r}\left(K^{11} r \frac{\partial C_s}{\partial r}\right) + \frac{1}{r^2}\frac{\partial}{\partial \theta}\left(K^{11}\frac{\partial C_s}{\partial \theta}\right) \right] \qquad (12)$$

The solute diffusion can change the solute concentration of the pore fluid, affecting pore pressure distribution. Therefore, based on the Fick's diffusion equation, solute concentration profile can be simulated, shown as:

$$\frac{\partial C_s}{\partial t} - \nabla (D^{eff} \cdot \nabla C_s) = 0 \qquad (13)$$

Meanwhile, considering the anisotropy of diffusion coefficient in shale formation, general equation for ion diffusion in shales can be transformed into polar coordinate, expressed as:

$$\frac{\partial C_s}{\partial t} = \frac{1}{r}\frac{\partial}{\partial r}\left(D_{ij}^{eff} r \frac{\partial C_s}{\partial r}\right) + \frac{1}{r^2}\frac{\partial}{\partial \theta}\left(D_{ij}^{eff} r \frac{\partial C_s}{\partial \theta}\right) \qquad (14)$$

The pore pressure propagation yields to its inner and external boundary of the borehole, which can be expressed as Eqs. (15), (16).

$$\begin{cases} C_s(r = r_w, \ \theta, \ t > 0) = C_m \\ p(r = r_w, \ \theta, \ t > 0) = p_i \end{cases} \qquad (15)$$

$$\begin{cases} C_s(r = \infty , \ \theta , \ t > 0) = C_o \\ p(r = \infty , \theta , \ t > 0) = p_o \end{cases} \quad (16)$$

In the initial condition, no pore pressure propagation occurs. Solute concentration and pore pressure are both equal to original value. Hence, the initial condition can be written as:

$$\begin{cases} C_s(r , \ \theta , \ t = 0) = C_o \\ p(r , \ \theta , \ t = 0) = p_o \end{cases} \quad (17)$$

With certain bedding plane angle ($a = 90°$) and $t = 144$ h, integrating these boundaries, initial conditions and transport equations, pore pressure distribution around wellbore can be obtained, shown as Fig. 8. It can be found out that with increasing radial distance, pore pressure increases firstly, then decreases to a stable level, which is close to original pore pressure. The propagation speed in isotropy condition has no change with circumferential angle. In contrast, due to hydraulic and diffusion anisotropy, propagation speed in layered formation is variable with circumferential angle. Since the maximums of hydraulic and diffusion are in the direction along bedding plane, pore pressure propagates faster and has small fluctuation at $\theta = 90°$ and $\theta = 270°$. On the other hand, pore pressure vertical to bedding plane needs to take a relatively longer distance to become stable value and has larger rising near wellbore, indicating that it is harder to have propagation at $\theta = 0°$ and $\theta = 180°$. This phenomenon can be explained by that high hydraulic and diffusion in bedding plane make this transport easily finished and reach balance, thus reducing changing range and propagation distance of pore pressure.

2.3 Seepage Stress Around Wellbore

The change of pore pressure distribution is able to modify seepage stress around wellbore. Based on the seepage stress equation in isotropy medium (Zhang et al. 2009), this equation has been modified by adding pore pressure anisotropy distribution ($p(r, \theta, t)$). As a result, seepage stress in shale formation can be expressed as:

$$\begin{cases} \sigma_r^s = \dfrac{a_b(1-2v)}{1-v} \dfrac{1}{r^2} \displaystyle\int_{r_w}^{r} (p(r,\theta,t) - p_o) r \, dr \\ \sigma_\theta^s = -\dfrac{a_b(1-2v)}{1-v} [\dfrac{1}{r^2} \displaystyle\int_{r_w}^{r} (p(r,\theta,t) - p_o) r \, dr \\ \qquad -(p(r,\theta,t) - p_o)] \\ \sigma_z^s = (\dfrac{a_b(1-2v)}{1-v})(p(r,\theta,t) - p_o) \end{cases} \quad (18)$$

In the Fig. 9, with $a = 90°$ and $t = 144$ h, seepage stresses around wellbore are illustrated on the basis of pore pressure propagation in Sect. 2.2. At the wall of wellbore ($r/r_w = 1$), seepages stresses are constant value. When the radial distance increases, due to the anisotropy effect, variations of seepage stresses are noticeable near wellbore area, reaching their maximum or minimum value at approximate $r/r_w = 1.1$. In the far field, seepage stresses restore to constant value. With increasing circumferential angle, circumferential stress grows firstly and then declines, having its peak point at $90°$. Radial and axis stress have opposite trend, reaching lowest point at $90°$.

2.4 Failure Mode and Strength Criterion

In combination with in situ stress components, pore pressure and seepage stress, stress state around wellbore in cylindrical coordinate can be written as (Liu et al. 2016):

$$\begin{cases} \sigma_r = \dfrac{r_w^2}{r^2} p_i + \tau_{xy}\left(1 + 3\dfrac{r_w^4}{r^4} - 4\dfrac{r_w^2}{r^2}\right)\sin 2\theta \\ \qquad + \dfrac{\sigma_{xx} - \sigma_{yy}}{2}\left(1 + 3\dfrac{r_w^4}{r^4} - 4\dfrac{r_w^2}{r^2}\right)\cos 2\theta \\ \qquad + \dfrac{\sigma_{xx} + \sigma_{yy}}{2}\left(1 - \dfrac{r_w^2}{r^2}\right) + \sigma_r^s \\ \sigma_\theta = -\dfrac{r_w^2}{r^2} p_i + \dfrac{\sigma_{xx} + \sigma_{yy}}{2}\left(1 + \dfrac{r_w^2}{r^2}\right) \\ \qquad - \dfrac{(\sigma_{xx} - \sigma_{yy})}{2}(1 + 3\dfrac{r_w^4}{r^4})\cos 2\theta \\ \qquad - \tau_{xy}(1 + 3\dfrac{r_w^4}{r^4})\sin 2\theta + \sigma_\theta^s \\ \sigma_z = \sigma_{zz} - 2v\left[(\sigma_{xx} - \sigma_{yy})\dfrac{r_w^2}{r^2}\cos 2\theta + 2\tau_{xy}\dfrac{r_w^2}{r^2}\sin 2\theta\right] + \sigma_z^s \\ \tau_{r\theta} = \tau_{xy}\left(1 + 2\dfrac{r_w^2}{r^2} - 3\dfrac{r_w^4}{r^4}\right)\cos 2\theta \\ \qquad + \dfrac{(\sigma_{xx} - \sigma_{yy})}{2}\left(1 + 2\dfrac{r_w^2}{r^2} - 3\dfrac{r_w^4}{r^4}\right)\sin 2\theta \\ \tau_{z\theta} = \tau_{yz}\left(1 + \dfrac{r_w^2}{r^2}\right)\cos\theta - \tau_{xz}(1 + \dfrac{r_w^2}{r^2})\sin\theta \\ \tau_{rz} = \tau_{xz}\left(1 - \dfrac{r_w^2}{r^2}\right)\cos\theta + \tau_{yz}(1 - \dfrac{r_w^2}{r^2})\sin\theta \end{cases} \quad (19)$$

Based on above stress state, principal stresses at the wall of wellbore can be expressed as Eq. (20). Besides, by performing comparison among 3 principal stresses, the maximum and minimum principal stress (σ_1 and σ_3) can be confirmed.

(a) Isotropy condition;

(b) Anisotropy condition;
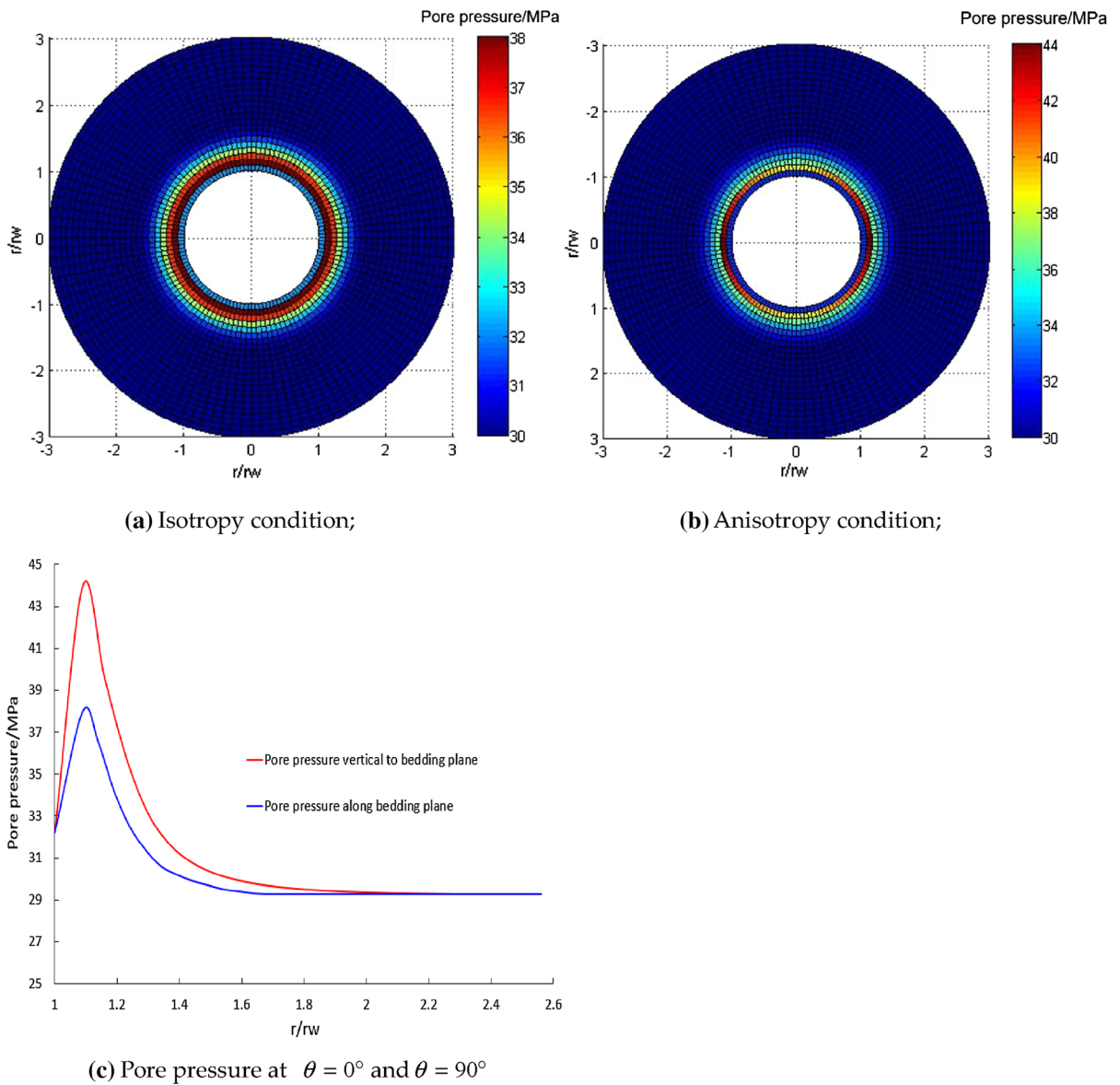

(c) Pore pressure at $\theta = 0°$ and $\theta = 90°$

Fig. 8 Pore pressure propagation around wellbore at $a = 90°$ and $t = 144$ h

$$\begin{cases} \sigma_i = \sigma_r \\ \sigma_j = \dfrac{\sigma_z - \sigma_\theta}{2} + \sqrt{(\dfrac{\sigma_\theta - \sigma_z}{2})^2 + \sigma_{\theta z}^2} \\ \sigma_k = \dfrac{\sigma_z - \sigma_\theta}{2} - \sqrt{(\dfrac{\sigma_\theta - \sigma_z}{2})^2 + \sigma_{\theta z}^2} \end{cases} \quad (20)$$

For shale failure mode, Jaeger's criterion gives the fact that shale has 2 types of shear failures, which are failure across rock matrix and along bedding plane (Lee et al. 2012). Accordingly, its schematic is shown in Fig. 10. Stress state at failure plane can be written as:

$$\tau = c_f + \sigma \tan \varphi_f \quad (21)$$

According to Eq. (21), the normal stress and shear stress at failure plane are expressed:

$$\begin{cases} \tau = \dfrac{\sigma_1 - \sigma_3}{2} \sin 2\beta_f \\ \sigma = \dfrac{\sigma_1 + \sigma_3}{2} + \dfrac{\sigma_1 - \sigma_3}{2} \cos 2\beta_f \end{cases} \quad (22)$$
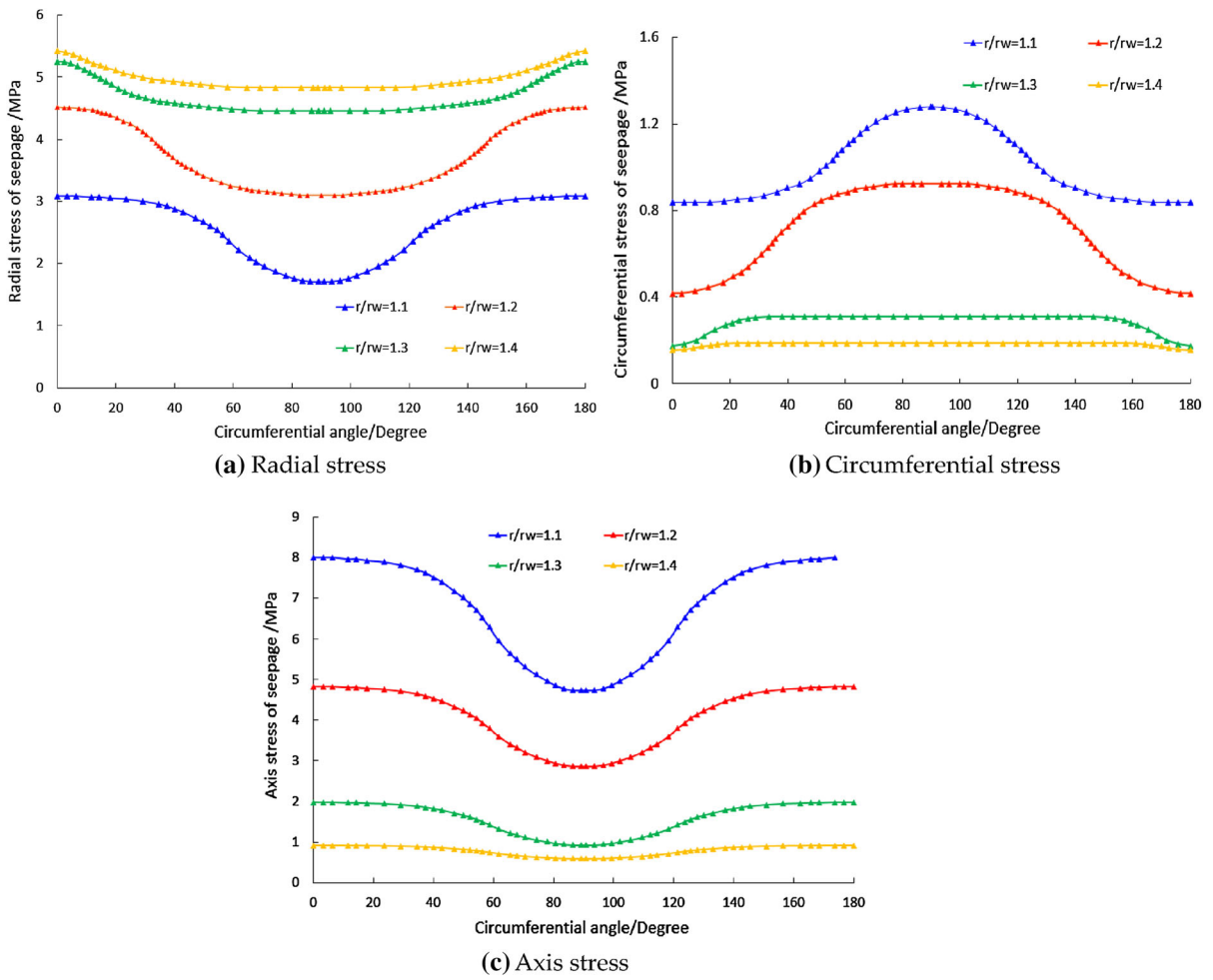
(a) Radial stress

(b) Circumferential stress

(c) Axis stress

Fig. 9 Seepage stress around wellbore
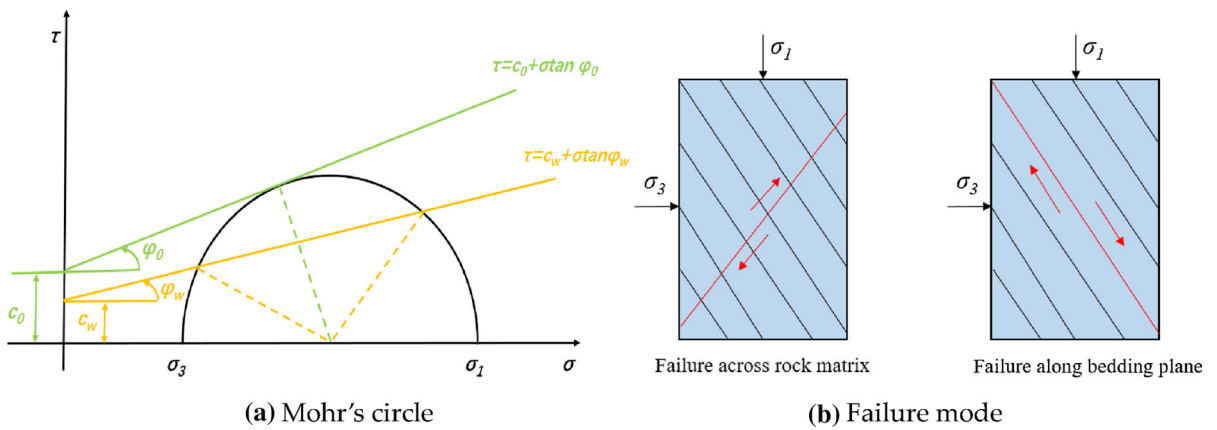

(a) Mohr's circle

(b) Failure mode

Fig. 10 Schematic of Jaeger's criterion

It is significant to note that failure plane could be plane along bedding plane or across matrix because 2 correspondingly failures exist (Fig. 10b). Therefore, inserting Eq. (22) into Eq. (21), the equation of shale strength criterion can be obtained, written as:

$$\begin{cases} \sigma_1 = \sigma_3 + \dfrac{2(c_w + \sigma_3 \tan \varphi_w)}{(1 - \tan \varphi_w \cot \beta_w) \sin 2\beta_w} & \text{Failure along bedding plane} \\[3mm] \sigma_1 = \sigma_3 + \dfrac{2(c_0 + \sigma_3 \tan \varphi_0)}{(1 - \tan \varphi_0 \cot \beta_0) \sin 2\beta_0} & \text{Failure across rock matrix} \end{cases} \tag{23}$$

β_f is the parameter of confirming failure mode, and its boundaries are shown in Eq. (24). Once $\beta_1 < \beta_f < \beta_2$ is satisfied, the shale will break along bedding plane. Otherwise, failure across rock matrix will happen.

$$\begin{cases} \beta_1 = \dfrac{\varphi_w}{2} + \dfrac{1}{2}\arcsin \dfrac{(\sigma_1 + \sigma_3 + 2c_w \cot \varphi_w) \sin \varphi_w}{\sigma_1 - \sigma_3} \\[3mm] \beta_2 = \dfrac{\pi}{2} + \dfrac{\varphi_w}{2} - \dfrac{1}{2}\arcsin \dfrac{(\sigma_1 + \sigma_3 + 2c_w \cot \varphi_w) \sin \varphi_w}{\sigma_1 - \sigma_3} \end{cases} \tag{24}$$

This criterion gives shale strength with variable bedding plane orientation, shown as Fig. 11. Curve made by this criterion is consistent with triaxial test data, proving its applicability. Additionally, in the middle of bedding plane orientation, clear strength reduction can be seen, indicating the shear failure along bedding plan will weaken wellbore stability and this failure type should be avoided in the drilling.
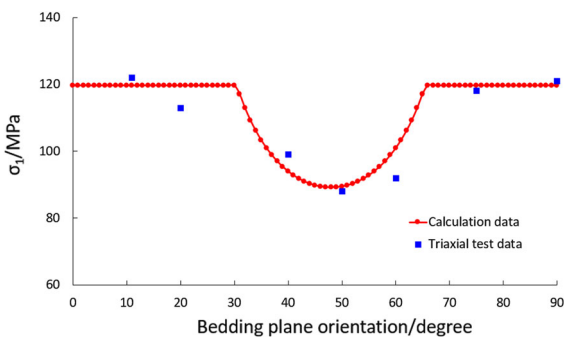

Fig. 11 Shale strength with bedding plane orientation

3 Influence Factors of Wellbore Stability in Shale Formation

Based on the model presented in the previous sections, factors influencing wellbore stability are analyzed in the following. Taking the horizontal well as an example, basic data are shown in Table 1. Also, calculated parameters for pore pressure and seepage stress are same as Table 2 in the Sect. 2.

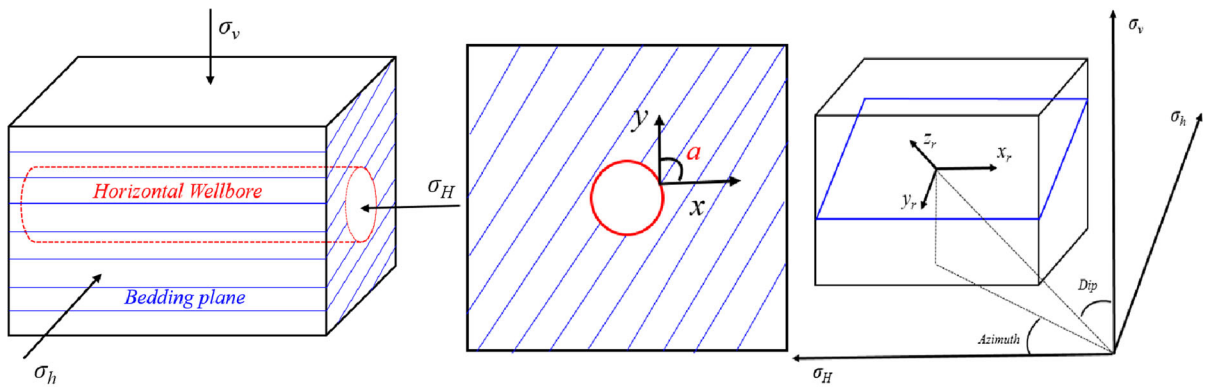### 3.1 Influence of Intersection Between Bedding Plane and Borehole

In shale reservoir, when horizontal well azimuth is confirmed, wellbore have different intersections with bedding plane occurrence, illustrated as Fig. 12. Different intersections will have variable bedding plane angle (a) in wellbore plane, changing the anisotropy around wellbore. As a result, failure region will be modified. For lamination formation, failure

Table 1 Input parameters

| No	Parameter	Value
1	Depth (m)	2834
2	Vertical in situ stress (MPa)	61.2
3	Maximum horizontal in situ stress (MPa)	52.5
4	Minimum horizontal in situ stress (MPa)	47.2
5	Mud pressure (MPa)	32.2
6	Cohesion of rock matrix (MPa)	20.7
7	Internal friction angle of rock matrix (°)	31.1
8	Cohesion of bedding plane (MPa)	14.2
9	Internal friction angle of bedding plane (°)	20.4
10	Poisson ratio along bedding plane	0.22
11	Poisson ratio vertical to bedding plane	0.25
12	Elastic modulus along bedding plane (GPa)	25.3
13	Elastic modulus vertical to bedding plane (GPa)	36.5

Table 2 Basic parameters for pore pressure propagation

No	Parameter	Value
1	Original pore pressure (MPa)	29.3
2	Mud pressure (MPa)	32.2
3	Porosity (%)	5.8
4	Radius of wellbore (m)	0.106
5	Biot coefficient	0.8
6	Solute concentration of fluid in formation (mol/L)	1.0
7	Solute concentration of drilling fluid (mol/L)	0.72
8	Hydraulic diffusion coefficient along bedding plane (m^3 s/kg)	5.5E-16
9	Hydraulic diffusion coefficient vertical to bedding plane (m^3 s/kg)	2.0E-16
10	Solute diffusion coefficient along bedding plane (m^2/s)	2.5E-14
11	Solute diffusion coefficient vertical to bedding plane (m^2/s)	1.6E-14
12	Membrane efficiency (m/Pa s)	3.2E-17
13	Compressibility of pore fluids (MPa^{-1})	1.24E-4
14	Temperature (°C)	105

(a) Horizontal wellbore in shale reservoir   (b) Wellbore plane   (c) Bedding plane occurrence

Fig. 12 Illustration of intersection between horizontal wellbore and bedding plane
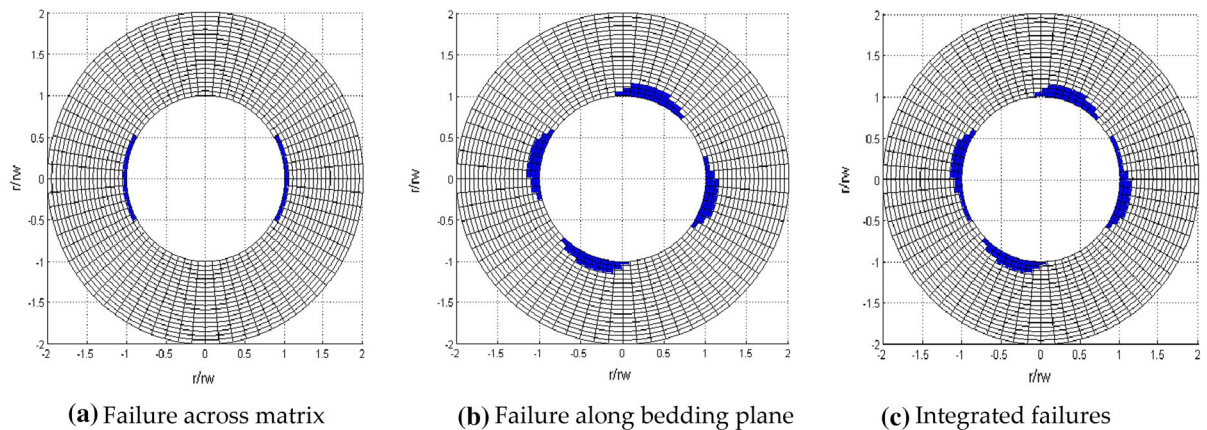
(a) Failure across matrix   (b) Failure along bedding plane   (c) Integrated failures

Fig. 13 Schematic of forming failure region around wellbore under different failure types
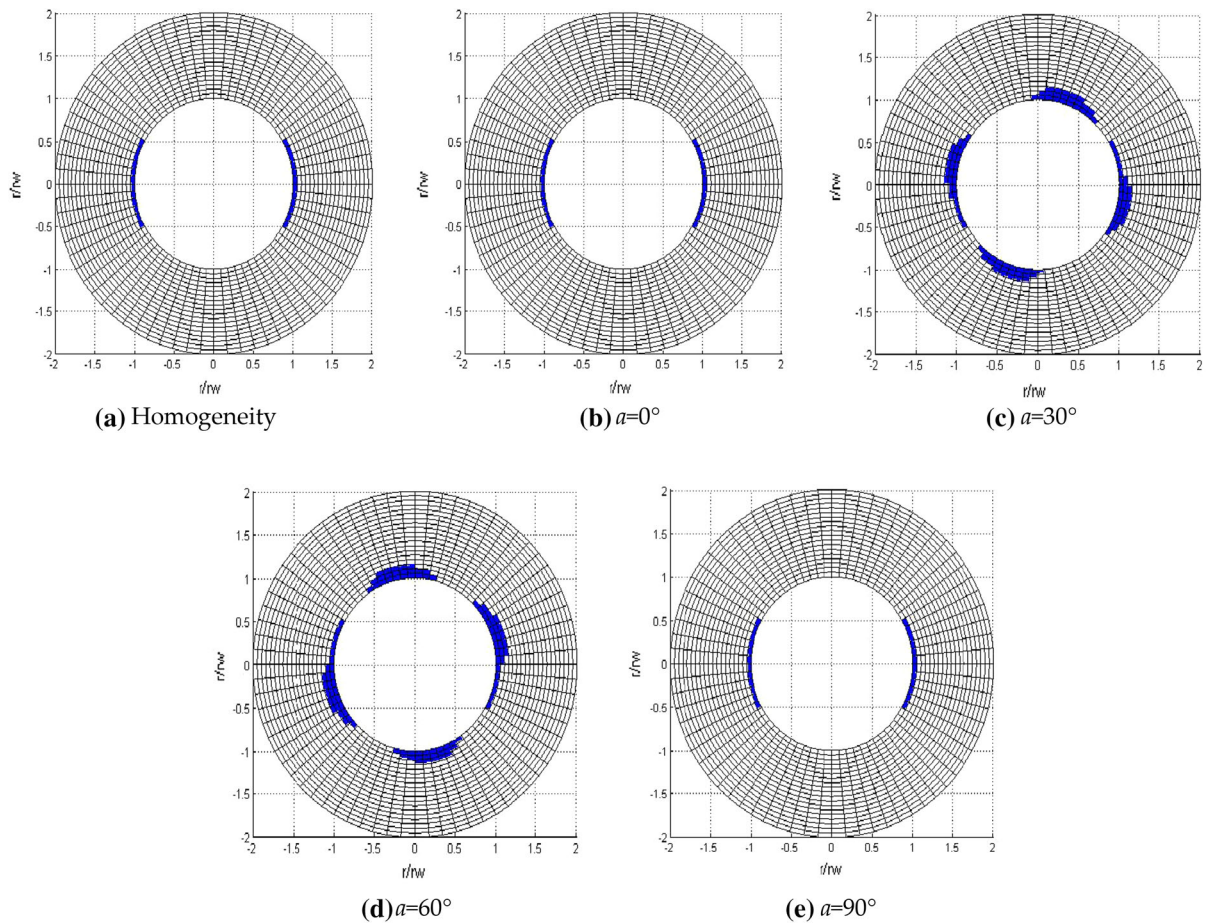
Fig. 14 Failure regions around wellbore with variable bedding plane angle at $t = 0$ h:

region is composed by two parts, which are regions of failure across matrix and failure along bedding plane. Its schematic is shown in Fig. 13. Based on this method, failure regions with different bedding plane angle have been calculated, shown in Fig. 14. We can find out that in homogeneity condition, only failure across rock matrix occurs and its failure region is typical two-lobed failure shape. In bedding plane condition, this failure region has no change in low and high bedding plane angle ($a = 0°$ and $a = 90°$), which indicates that shear failure along bedding plane doesn't happen in this scenario and wellbore stability is depended on rock matrix strength. On the other hand, Fig. 14c, d, where $a = 30°$ and $a = 60°$, illustrate that failure region clearly increases and becomes four-lobed failure shape, suggesting shear failure along bedding plane occurs and aggravates the instability.

3.2 Influence of Pore Pressure Propagation and Seepage Stress

As discussed earlier, pore pressure propagation and seepage stress are indispensable part of stress state around wellbore. This part is not included in the Sect. 3.1 since no water and ion transport happens at $t = 0$ h. Therefore, to clarify this influence, failure region with pore pressure propagation and seepage have been computed ($t = 144$ h), shown in Fig. 15. Based on the comparison between Figs. 14 and 15, it is evident that failure region is enlarged due to pore pressure propagation and seepage stress. Besides, this increment is variable with different bedding plane angles. Although failure region is increased, region shapes are not modified. Shape is still two-lobed in the low and high angle, four-lobed in middle angle, suggesting that pore pressure propagation and seepage

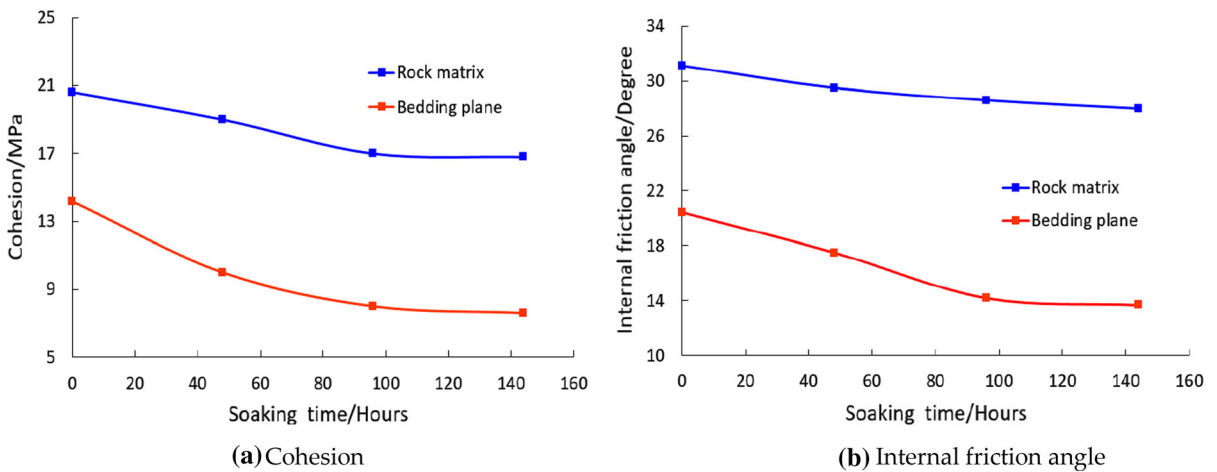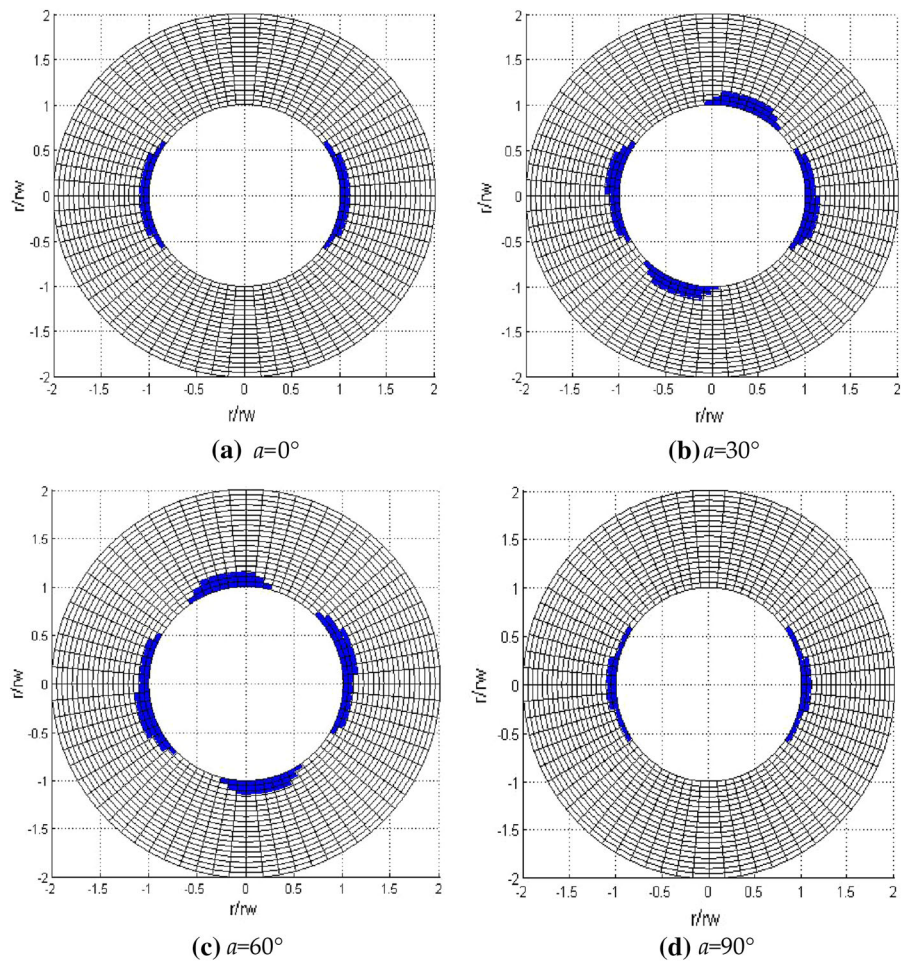**Fig. 15** Failure region around wellbore with pore pressure propagation and seepage stress at $t = 144$ h

(a) $a=0°$

(b) $a=30°$

(c) $a=60°$

(d) $a=90°$

(a) Cohesion

(b) Internal friction angle

Fig. 16 Mechanical parameters in different soaking time

stress only increase collapse area and cannot change the failure mode.

3.3 Influence of Drilling Fluid

In drilling operation, when shale interacts with drilling fluid, hydration effect will reduce shale strength and impair wellbore stability (Manshad et al. 2014). To analyse drilling fluid influence, shale strength is firstly measured on the basis of shear test, shown in Fig. 16. With increasing soaking time, strength of rock matrix and bedding plane both show decreasing trend. Especially, compared to rock matrix, the strength decline of bedding plane is bigger, indicating bedding plane has strong sensitivity to drilling fluid. This strong sensitivity is caused by high permeability of bedding plane, making fluid invasion much easily through bedding plane.

Under the assumption that rock near wellbore has same strength in Fig. 16, failure region with drilling time is investigated, shown in Figs. 17, 18 and 19. Also, the failure region without drilling fluid impact ($t = 0$ h) has already been illustrated in Sect. 3.1 (Fig. 14). With increasing drilling time, because of the strength decline induced by hydration, failure region has clear increment. According to the change of failure region, it can be seen that region increment is larger in the initial stage (0–96 h), and become stable in the later period. More importantly, in later stage of drilling, drilling fluid effect not only increase failure region, but also change failure mode. At $a = 0°$ and $a = 90°$, when drilling time becomes 96 h, failure region has tremendously growth and transforms from two-lobed to four-lobed shape, indicating shear failure along bedding plane occurs. Comparing these failure regions, we can find out that the intersection with middle bedding plane angle has larger failure region

and can be considered as the most unstable scenario for drilling in shale reservoir.

4 Conclusion

In this study, we have fully consideration for shale anisotropy in rock mechanical properties, hydraulic coefficient, diffusion coefficient, etc. Correspondingly, calculated equations for shale strength, in situ stress components, pore pressure propagation and seepage stresses in anisotropic medium have been established. Subsequently, in combination with these equations, a new analytical model has been developed to analyze failure region and evaluate wellbore stability. For this analytical model, it is built on these conditions and assumptions: (1) shale formation is linear elastic and transversely isotropic. (2) flow of fluid around wellbore accords with Darcy laws. (3) diffusion around wellbore accords with Fick law. (4) wellbore inclined degree is 90° (i.e., horizontal wellbore). Finally, based on this model, we can come to the following conclusions:

(1) For in situ stress components, because of transversely isotropy with bedding plane, elastic parameters and bedding plane occurrence can affect in situ stress components distribution, making it different from homogeneity situation. Meanwhile, due to hydraulic and diffusion coefficient anisotropy, transport speed in layered formation is variable with circumferential angle. For the direction along bedding plane having the maximums of hydraulic and diffusion coefficient, pore pressure propagates faster and has small fluctuation. On the other hand, pore pressure vertical to bedding plane needs to
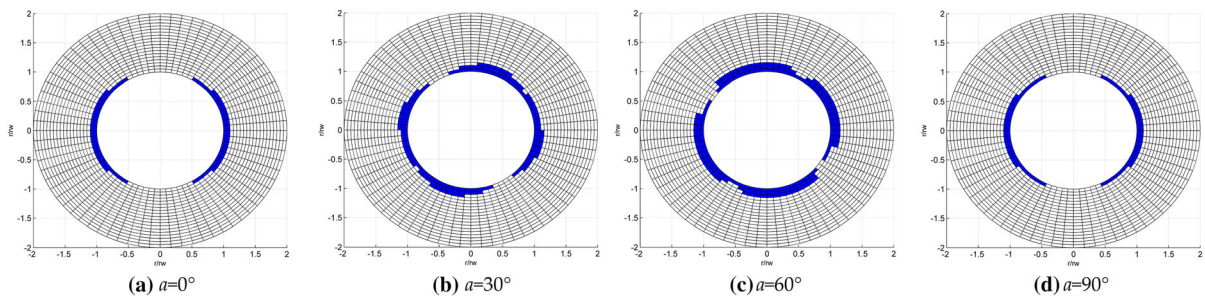

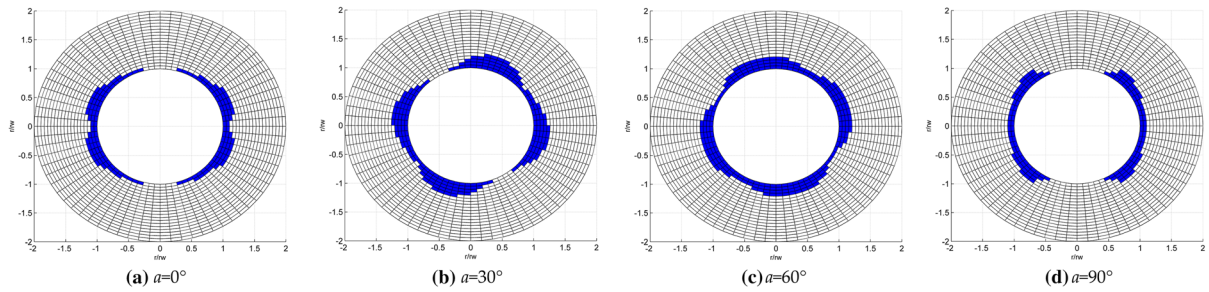**Fig. 17** Failure region in different drilling time at 48 h"

Fig. 18 Failure region in different drilling time at 96 h
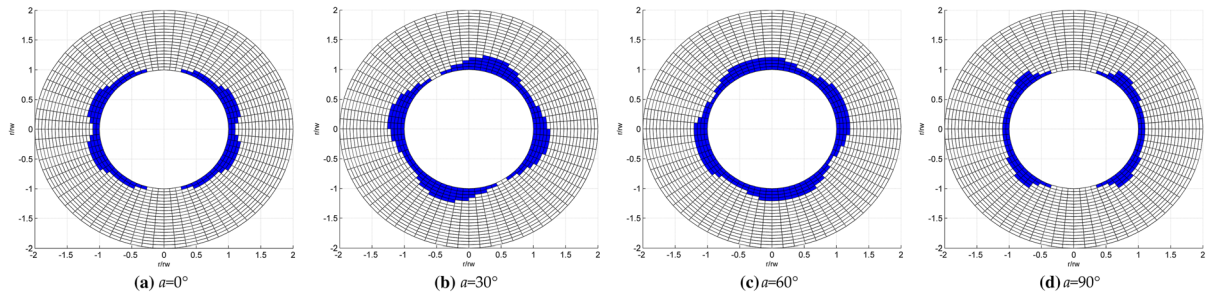

Fig. 19 Failure region in different drilling time at 144 h

take a longer distance to become stable and has larger rising in the vicinity of wellbore.

(2) The pore pressure propagation can change seepage stress distribution. At the wall of wellbore, seepages stresses are constant. When the radial distance increases, due to the anisotropy effect, variation of seepage stresses is noticeable near wellbore area. In the area away from wellbore, seepage stresses come back to a stable level. With increasing circumferential angle, circumferential stress grows firstly and then declines, having its peak point at 90°. In contrast, radial and axis stress have the opposite tendency.

(3) Shale strength is associated with bedding plane orientation. This changing trend is obtained on the basis of single weak plane criterion, and verified by triaxial test data. Based on that, in the middle of bedding plane orientation, obvious strength reduction can be noticed, indicating the shear failure along bedding plan occurs. This phenomenon suggests that this shear failure can weaken wellbore stability and should be avoided in the drilling.

(4) When horizontal wellbore has different intersections with bedding plane, varying bedding

plane angles exist in wellbore plane, changing the failure region around wellbore. In homogeneity condition with only failure across rock matrix, failure region is typical two-lobed failure shape. Considering the existence of bedding plane, this failure region has no change in low and high bedding plane angle, indicating failure mode has no change and wellbore stability is merely relied on rock matrix strength. Whereas, in the middle a, failure region clearly increases and becomes four-lobed failure shape, suggesting shear failure along bedding plane occurs and aggravates the instability. Meanwhile, failure region is enlarged by pore pressure propagation and seepage stress. However, influences of pore pressure and seepage stress are not enough to affect failure mode.

(5) Under the influence of drilling fluid, strength of rock matrix and bedding plane both show decreasing trend. Especially, bedding plane is more sensitive to drilling fluid, having lager strength decline. With increasing drilling time, failure region has clear increment. This increment is large in the initial stage and then becomes stable in the later stage. In particular, after 96 h, drilling fluid effect can change

failure mode from failure across rock matrix to failure along bedding plane. Correspondingly, failure regions of two-lobed failure shape at low and high bedding plane angle gradually become four-lobed. Comparing these failure regions, we can conclude that intersection with middle bedding plane angle is the most unstable scenario since it has largest failure region.

References

Aadnoy BS (1987) Stresses around horizontal boreholes drilled in sedimentary rocks. J Petrol Sci Eng 2:349–360

Al-Ajmi AM (2012) Mechanical stability of horizontal wellbore implementing Mogi-Coulomb law. Adv Petrol Explor Dev 4(2):28–36

Amadei B (1984) In Situ, stress measurements in anisotropic rock. Int J Rock Mech Min Sci Geomech Abstr 21(6):327–338

Chen G, Chenevert ME, Sharma MM, Yu M (2003) A study of wellbore stability in shales including poroelastic, chemical, and thermal effects. J Petrol Sci Eng 38:167–176

Chen P, Ma T, Xia H (2015) A collapse pressure prediction model for horizontal shale gas wells with multiple weak planes. Nat Gas Ind B 2(1):101–107

Deville JP, Fritz B, Jarrett M (2011) Development of water-based drilling fluids customized for shale reservoirs. SPE Drill Compl 26(4):484–491

Ding Y, Luo P, Liu X, Liang L (2018) Wellbore stability model for horizontal wells in shale formations with multiple planes of weakness. J Nat Gas Sci Eng 52:334–347

Dokhani V, Yu M, Takach NE, Bloys B (2015) The role of moisture adsorption in wellbore stability of shale formations: mechanism and modeling. J Nat Gas Sci Eng 27:168–177

Dokhani V, Yu M, Bloys B (2016) A wellbore stability model for shale formations: accounting for strength anisotropy and fluid induced instability. J Nat Gas Sci Eng 32:174–184

Ekbote S, Abousleiman Y (2006) Porochemoelastic solution for an inclined borehole in a transversely isotropic formation. J Eng Mech 132(7):754–763

Gupta D, Zaman M (1999) Stability of boreholes in a geologic medium including the effects of anisotropy. Appl Math Mech 20(8):16–45

He S, Zhou J, Chen Y, Li X, Tang M (2017) Research on wellbore stress in under-balanced drilling horizontal wells considering anisotropic seepage and thermal effects. J Nat Gas Sci Eng 45:338–357

Kanfar MF, Chen Z, Rahman SS (2017) Analyzing wellbore stability in chemically-active anisotropic formations under thermal, hydraulic, mechanical and chemical loadings. J Nat Gas Sci Eng 41:93–111

Lee H, Ong SH, Azeemuddin M, Coodman H (2012) A wellbore stability model for formations with anisotropic rock strengths. J Petrol Sci Eng 96:109–119

Lekhnitskii SG (1963) On the problem of the elastic equilibrium of an anisotropic strip. J Appl Math Mech 27(1):197–209

Lomba RFT, Chenevert ME, Sharma MM (2000) The ion-selective membrane behavior of native shales. J Petrol Sci Eng 25:9–23

Liang C, Chen M, Jin Y, Liu Y (2014) Wellbore stability model for shale gas reservoir considering the coupling of multi-weakness planes and porous flow. J Nat Gas Sci Eng 21:364–378

Liu M, Jin Y, Lu Y, Chen M, Hou B, Chen W, Wen X, Yu X (2016) A wellbore stability model for a deviated well in a transversely isotropic formation considering poroelastic effects. Rock Mech Rock Eng 49(9):1–16

Liu X, Ding Y, Ranjith PG, Luo P (2019) Hydration index and hydrated constitutive model of clay shale using acoustic frequency spectrum. Energy Sci Eng 7(5):1748–1766

Ma T, Chen P (2014) Study of meso-damage characteristics of shale hydration based on CT scanning technology. Petrol Explor Dev 41(2):249–256

Ma T, Chen P (2015) A wellbore stability analysis model with chemical-mechanical coupling for shale gas reservoirs. J Nat Gas Sci Eng 26:72–98

Manshad AK, Jalalifar H, Aslannejad M (2014) Analysis of vertical, horizontal and deviated wellbores stability by analytical and numerical methods. J Petrol Explor Prod Technol 4(4):359–369

Meier T, Rybacki E, Backers T, Dresen G (2015) Influence of bedding angle on borehole stability: a laboratory investigation of transverse isotropic oil shale. Rock Mech Rock Eng 48(4):1535–1546

Mody FK, Hale AH (1993) Borehole-stability model to couple the mechanics and chemistry of drilling-fluid/shale interactions. J Petrol Technol 45(11):1093–1101

Qian J, Wang J, Li S (2003) Oil shale development in China. Oil Shale 20(3):356–359

Rizzo FJ, Shippy DJ (1970) A method for stress determination in plane anisotropic elastic bodies. J Compos Mater 4(1):36–61

Wang Q, Zhou Y, Wang G, Jiang HW, Liu YS (2012) A fluid-solid-chemistry coupling model for shale wellbore stability. Petrol Explor Dev 39(4):508–513

Yang TH, Jia P, Shi WH, Wang PT, Liu HL, Yu QL (2014) Seepage–stress coupled analysis on anisotropic characteristics of the fractured rock mass around roadway. Tunn Undergr Space Technol 43(7):11–19

Yuan JH, Luo DK, Feng LY (2015) A review of the technical and economic evaluation techniques for shale gas development. Appl Energy 148:49–65

Yu M (2002) Chemical and thermal effects on wellbore stability of shale formations. J Petrol Technol 54(2):51–51

Yu M, Chenevert ME, Sharma MM (2003) Chemical–mechanical wellbore instability model for shales: accounting for solute diffusion. J Petrol Sci Eng 38:131–143

Zhang L, Shan B, Zhao Y, Tang H (2018) Comprehensive seepage simulation of fluid flow in multi-scaled shale gas reservoirs. Transp Porous Media 121(2):263–288

Zhang C, Yu Y, Zhao Q (2009) Seepage-stress elastoplastic coupling model of heterogeneous coal and numerical simulation. Rock Soil Mech 30(9):2837–2842

Zhong HY, Qiu ZS, Huang WA, Cao J (2011) Shale inhibitive properties of polyether diamine in water-based drilling fluid. J Petrol Sci Eng 78:510–515

Zhou J, He S, Tang M, Huang Z, Chen Y, Chi J, Zhu Y, Yuan P (2018) Analysis of wellbore stability considering the effects of bedding planes and anisotropic seepage during drilling horizontal wells in the laminated formation. J Petrol Sci Eng 170:507–524

Zoback MD, Moos D, Mastin L, Anderson RN (1985) Well bore breakouts and in situ stress. J Geophy Res Solid Earth 90(B7):5523–5530